

The NLRP3 inflammasome functions as a negative regulator of tumorigenesis during colitis-associated cancer

Irving C. Allen,¹ Erin McElvania TeKippe,² Rita-Marie T. Woodford,³ Joshua M. Uronis,⁴ Eda K. Holl,³ Arlin B. Rogers,⁵ Hans H. Herfarth,^{4,6} Christian Jobin,^{4,7} and Jenny P.-Y. Ting^{1,2,3,4}

¹Lineberger Comprehensive Cancer Center, ²Department of Microbiology and Immunology, ³School of Dentistry, Oral Biology Program, ⁴Department of Medicine, Center for Gastrointestinal Biology and Disease, ⁵Department of Pathology and Laboratory Medicine, ⁶Department of Medicine, Division of Gastroenterology and Hepatology, ⁷Department of Medicine, Pharmacology, the University of North Carolina at Chapel Hill, Chapel Hill, NC 27599

Colitis-associated cancer (CAC) is a major complication of inflammatory bowel diseases. We show that components of the inflammasome are protective during acute and recurring colitis and CAC in the dextran sulfate sodium (DSS) and azoxymethane + DSS models. Mice lacking the inflammasome adaptor protein PYCARD (ASC) and caspase-1 demonstrate increased disease outcome, morbidity, histopathology, and polyp formation. The increased tumor burden is correlated with attenuated levels of IL-1 β and IL-18 at the tumor site. To decipher the nucleotide-binding domain, leucine-rich-repeat-containing (NLR) component that is involved in colitis and CAC, we assessed *Nlrp3* and *Nlr4* deficient mice. *Nlrp3*^{-/-} mice showed an increase in acute and recurring colitis and CAC, although the disease outcome was less severe in *Nlrp3*^{-/-} mice than in *Pycard*^{-/-} or *Casp1*^{-/-} animals. No significant differences were observed in disease progression or outcome in *Nlr4*^{-/-} mice compared with similarly treated wild-type animals. Bone marrow reconstitution experiments show that *Nlrp3* gene expression and function in hematopoietic cells, rather than intestinal epithelial cells or stromal cells, is responsible for protection against increased tumorigenesis. These data suggest that the inflammasome functions as an attenuator of colitis and CAC.

CORRESPONDENCE

Jenny P.-Y. Ting:
panyun@med.unc.edu

Abbreviations used: AOM, azoxymethane; ASC/PYCARD, Apoptotic Speck protein containing a CARD; CAC, colitis-associated cancer; CRC, colorectal cancer; DAMP, damage-associated molecular pattern; DSS, dextran sulfate sodium; HAI, Histological Activity Index; IBD, inflammatory bowel disease; NLR, nucleotide-binding domain, leucine-rich-repeat-containing; TLR, Toll-like receptor; UC, ulcerative colitis.

It is now commonly accepted that inflammation contributes to the initiation, promotion, and progression of tumor development. Although it has long been speculated that inflammation is associated with cancer, the underlying mechanisms have been elusive and are only now beginning to be defined (Coussens and Werb, 2002). One of the best clinically characterized examples of the association between inflammation and carcinogenesis is the development of colon cancer in patients suffering from ulcerative colitis (UC), which is a common form of inflammatory bowel disease (IBD). UC affects ~1 person per 600 in the US, and it is defined by characteristic ulcers observed in the colon. Patients suffering from UC demonstrate a significantly increased risk of colorectal cancer (CRC), which seems to be associated with both the duration of the disease and the degree of mucosal inflammation (Eaden

et al., 2001). CRC is the third most common form of cancer in the Western hemisphere and accounts for 655,000 deaths per year worldwide. A common denominator for both UC and colon cancer is the activation of pathways associated with inflammation.

Two families of innate immune receptors, the Toll-like receptors (TLRs) and the nucleotide-binding domain, leucine-rich-repeat-containing (NLR) proteins, have emerged as essential mediators of gastrointestinal inflammation and homeostasis (Akira et al., 2006; Franchi et al., 2006). The NLRs mediate host immune response to a myriad of pathogen-associated molecular patterns, including bacteria,

© 2010 Allen et al. This article is distributed under the terms of an Attribution-Noncommercial-Share Alike-No Mirror Sites license for the first six months after the publication date (see <http://www.rupress.org/terms>). After six months it is available under a Creative Commons License (Attribution-Noncommercial-Share Alike 3.0 Unported license, as described at <http://creativecommons.org/licenses/by-nc-sa/3.0/>).

fungi, and viruses, as well as damage-associated molecular patterns (DAMPs), including uric acid, alum salt, silica, and reactive oxygen species (Cassel et al., 2009). Among the TLR family, various members (TLR2, TLR4, TLR5, and TLR9) and their adaptor protein MyD88 have been shown to be involved in innate immune signaling pathways associated with gastrointestinal inflammation and tumorigenesis in both humans and mice (Fukata and Abreu, 2009). Similar to the TLRs, members of the NLR family have also been implicated as modulators of gastrointestinal inflammation, including NOD2, which is the prototypical NLR associated with IBD (Ogura et al., 2001). However, the vast majority of NLR family members have yet to be assessed in models of gastrointestinal inflammation and tumorigenesis.

The processing and release of proinflammatory cytokines and chemokines, including IL-1 β and IL-18, is fundamental to proper innate immune responses to pathogens and environmental insults in the gastrointestinal system. Genetic association studies showed that polymorphisms in the IL-1 β gene cluster significantly increase the risk of developing a variety of cancers, including gastric cancer (Barber et al., 2000; El-Omar et al., 2001). IL-1 β levels are significantly altered in patients suffering from either acute or chronic gastrointestinal inflammation and have been implicated in tumor angiogenesis, progression, and metastasis (Bioque et al., 1995; Casini-Raggi et al., 1995). In many circumstances, IL-1 β and IL-18 processing is dependent on the NLR protein, NLRP3, which associates with the NLR adapter protein, Apoptotic Speck protein containing a CARD (ASC/PYCARD), to recruit procaspase-1. This complex is referred to as the inflammasome,

and leads to the processing of procaspase-1 into caspase-1 (Agostini et al., 2004). Caspase-1 is responsible for the subsequent cleavage of the IL-1 β /IL-18 precursor into their functional forms. In addition to NLRP3, other NLRs, including NLRP1, NLRC4, and NAIP, also function in caspase-1 activation and IL-1 β production through the formation of other inflammasomes in response to distinct sets of stimuli (Mariathasan et al., 2004).

Although studies in humans and mice have found a significant role for IL-1 β in tumorigenesis, the roles of the inflammasome components have not been studied. In this study, we show that components of the inflammasome have a profound protective influence on colitis and colitis-associated cancer (CAC). This study is the first to address the role of NLR inflammasomes in CAC and demonstrates a protective role for PYCARD, caspase-1, and NLRP3 against CAC development.

RESULTS

NLR inflammasome components attenuate acute and recurring gastrointestinal inflammation during experimentally induced colitis

We first sought to assess the role of the NLRP3 inflammasome in acute and recurring models of gastrointestinal inflammation, without the confounding effects of tumor development. The dextran sulfate sodium (DSS) model has been shown to recapitulate many of the clinical observations associated with UC in humans (Neufert et al., 2007). In the acute model, mice were challenged with 5% DSS for 6 d and survival was assessed for 14 d (Fig. 1 A). Under these conditions,

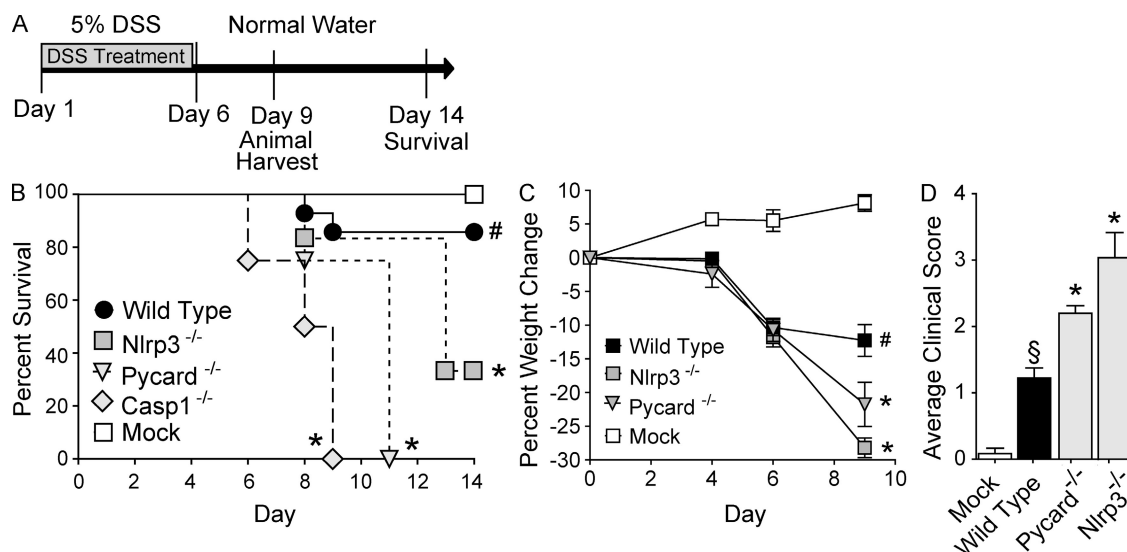


Figure 1. NLR inflammasome components attenuate acute ulcerative colitis. (A) Schematic of the acute model of DSS-induced ulcerative colitis. (B) Kaplan-Meier plot of WT, *Nlrp3*^{-/-}, *Pycard*^{-/-}, and *Casp1*^{-/-} mouse survival. (C) Weight loss of WT, *Nlrp3*^{-/-}, and *Pycard*^{-/-} mice. (D) Clinical parameters (weight loss, stool consistency, bleeding) of indicated mice. Data shown are representative of at least three independent experiments and depict the mean \pm SEM. The symbols # and § indicate $P < 0.05$ and $P < 0.01$, respectively, between the mock- and DSS-treated WT; * indicates $P < 0.05$ between the DSS-treated gene-deficient strains compared with DSS-treated WT. WT mock, $n = 4$; DSS-treated WT, $n = 14$; *Pycard*^{-/-}, $n = 4$; *Nlrp3*^{-/-}, $n = 6$; *Casp1*^{-/-}, $n = 4$. *Casp1*^{-/-} animals were highly sensitive to the acute administration of DSS and were not subjected to additional monitoring described in C and D for humane reasons.

the *Casp1*^{-/-} and *Pycard*^{-/-} mice demonstrated a significant decrease in survival, with all animals requiring euthanasia by days 9 and 11, respectively (Fig. 1 B). Although not as dramatic as the *Casp1*^{-/-} and *Pycard*^{-/-} mortality data, a significant decrease in survival was also observed for *Nlrp3*^{-/-} mice compared with the WT mice (Fig. 1 B). It should be noted that mice deficient in caspase-1 demonstrated a very severe phenotype in the acute colitis model and additional experiments were required to be halted because of humane reasons. Weight loss is typically considered a surrogate marker of morbidity and was assessed throughout the course of the DSS model. Consistent with the mortality data, the *Nlrp3*^{-/-} and *Pycard*^{-/-} mice demonstrated significant weight loss compared with the WT animals (Fig. 1 C). Moribund mice were euthanized at day 9. The clinical score was measured using a semiquantitative scoring system designed to evaluate the hallmark features of gastrointestinal disease in mice (weight loss, stool consistency, and rectal bleeding; Siegmund et al., 2001). Consistent with increased morbidity and mortality, *Pycard*^{-/-} and *Nlrp3*^{-/-} mice presented with clinical features associated with enhanced gastrointestinal disease (Fig. 1 D). Together, these data suggest a protective role for both *Pycard* and *Nlrp3* in acute colitis induced by DSS.

We next assessed the roles of *Pycard*, *Casp1*, and *Nlrp3* in a recurring colitis model. These mice were subjected to three rounds of DSS treatment (2.5%) over the course of 60 d (Fig. 2 A; Neufert et al., 2007). After the completion of the recurring model, *Pycard*^{-/-} *Casp1*^{-/-} and *Nlrp3*^{-/-} mice showed increased inflammation and gastrointestinal disease, although the *Nlrp3*^{-/-} mice had a more subtle disease. Increased weight loss was observed in all DSS-treated mice, but after the first round of DSS treatment (between days 8 and 10), *Pycard*^{-/-} (-10.9%) and *Nlrp3*^{-/-} (-9.0%) animals exhibited more severe weight loss than WT controls (-2.3%; Figs. 2, B and C). Both strains recovered after this initial decrease, and no other significant differences in weight loss were observed during subsequent DSS administrations. However, similar to the findings of the acute colitis study, *Casp1*^{-/-} animals were also highly sensitive to the recurring colitis model, with the majority requiring euthanasia by day 41 (Fig. 2 D). All DSS-challenged mice presented with significantly increased features of gastrointestinal disease, but *Pycard*^{-/-}, *Casp1*^{-/-}, and *Nlrp3*^{-/-} mice demonstrated significantly elevated clinical scores (0.67, 0.83, and 0.73, respectively) compared with the WT animals (0.22; Fig. 2 E). As an additional assessment of disease status, colon length was used to correlate with disease severity. Truncated colons were observed in all DSS-treated mice, but colons harvested from *Pycard*^{-/-} (6.1 cm) and *Casp1*^{-/-} (6.4 cm) mice showed significant truncation compared with the WT (7.7 cm) or *Nlrp3*^{-/-} mice (7.8 cm; Fig. 2 F and Fig. S1 A).

In the UC model, the Histological Activity Index (HAI) is a composite score based on individual scores of inflammation, epithelial defects, crypt atrophy, and the area involved in disease in the mid and distal colon (Meira et al., 2008). All DSS-treated animals demonstrated a significant increase in

the overall HAI score compared with mock-treated WT mice (Fig. 2 G). No significant differences in histopathology were observed between the DSS-treated WT and *Nlrp3*^{-/-} mice; however, *Pycard*^{-/-} and *Casp1*^{-/-} animals demonstrated significantly increased HAI scores compared with the other genotypes (Fig. 2 G). Characterization of the individual HAI components including inflammation, epithelial defects, crypt atrophy, and area involved in disease is depicted in Fig. S1 (B–E). These data indicate a stronger protective role of PYCARD and caspase-1 than NLRP3 in recurring colitis. Together, these data suggest that inflammasome components attenuate both acute and recurring models of colitis. Because of the ultimate interest in colitis-associated tumorigenesis, we restricted the rest of this study to the recurring colitis model.

The inflammasome adaptor protein PYCARD and caspase-1 are required for tumor reduction in CAC

We next sought to assess the role of both PYCARD and caspase-1 in the development of inflammation-driven colon tumorigenesis. In humans, CRC can develop either spontaneously or as a complication of IBD. Of the chemical carcinogens used in rodent CRC models, the majority of studies have used azoxymethane (AOM). Although AOM alone exerts colonotropic carcinogenicity, inflammation-dependent tumor development can be assessed by combining AOM with the UC model (Neufert et al., 2007).

To evaluate the role of NLR inflammasomes in the initiation and progression of CAC, *Pycard*^{-/-} and *Casp1*^{-/-} mice were subjected to an AOM/DSS recurring inflammation-driven colon tumorigenesis model. This model differs from the recurring colitis model in that the carcinogen AOM is given before DSS treatment (Fig. 3 A; Neufert et al., 2007). No overt phenotype, spontaneous gastrointestinal inflammation or tumorigenesis has been reported by others, nor observed by us, in naive *Pycard*^{-/-}, *Casp1*^{-/-}, and *Nlrp3*^{-/-} animals. After AOM and the completion of the first two DSS challenges, a dramatic increase in the number of moribund *Casp1*^{-/-} and *Pycard*^{-/-} mice was observed compared with similarly treated WT animals (Fig. 3 B). The moribund *Casp1*^{-/-} (87.5%) and *Pycard*^{-/-} (77.8%) mice were humanely euthanized between days 29 and 46. As in the experimental colitis model, weight loss was assessed at least five times per week throughout the inflammation-driven colon tumorigenesis model. The majority of *Casp1*^{-/-} animals demonstrated significantly increased sensitivity to repeated challenges with DSS, with a drastic decrease in body weight (range, -15.7 to -42.7%) observed after the completion of two rounds of treatment (Fig. 3 C). *Pycard*^{-/-} mice demonstrated significantly increased weight loss starting from day 15, which lasted through the duration of treatment (Day 29 = -16.10 ± 5.64%) compared with the WT animals (Day 29 = -0.89 ± 1.54; Fig. 3 D). The majority of *Casp1*^{-/-} and *Pycard*^{-/-} mice required euthanasia for humane reasons between days 29 and 38. Hence, no additional weight loss data were collected for these animals beyond the time points shown. Consistent with changes in mortality and morbidity,

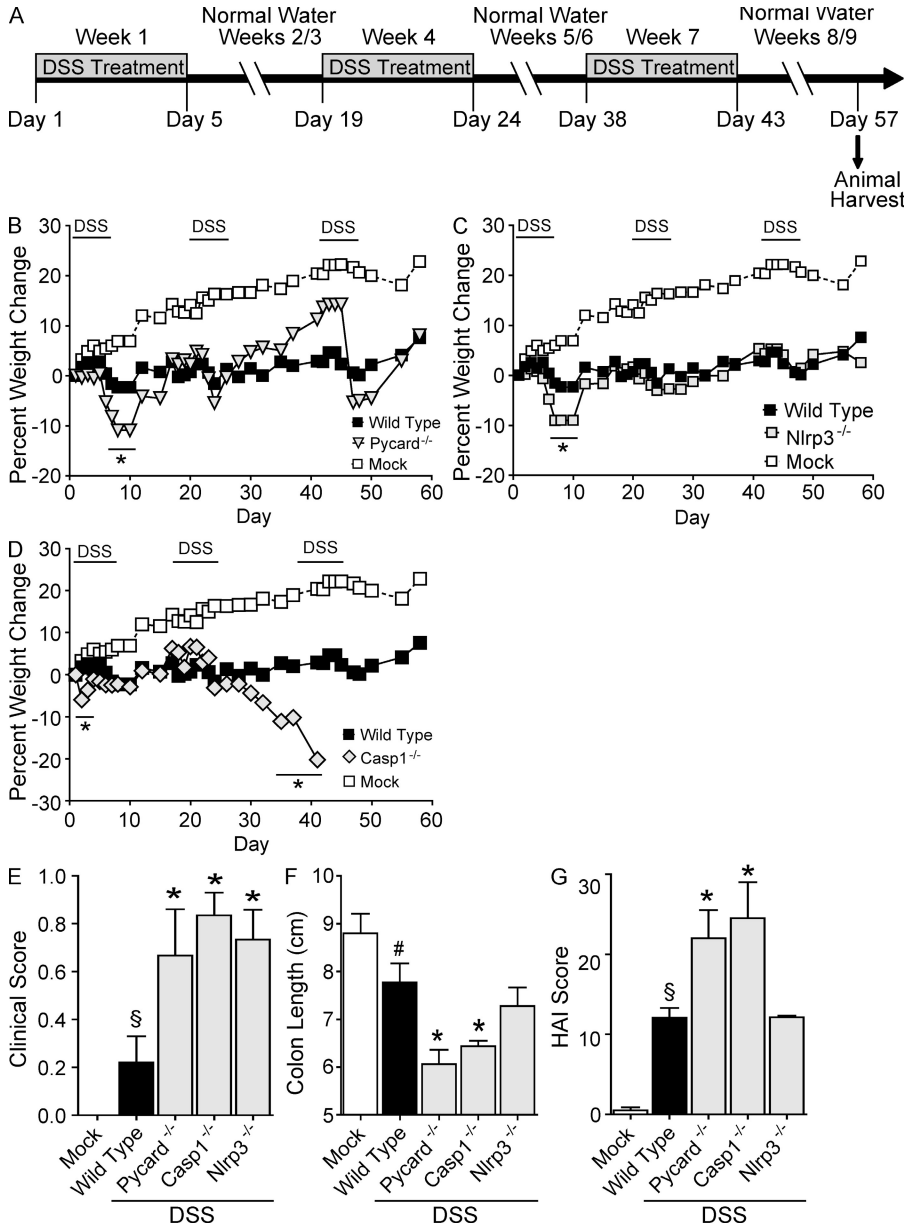


Figure 2. NLR inflammasome components attenuate recurring ulcerative colitis. (A) Schematic of the recurring model of DSS-induced ulcerative colitis. (B–D) Weight loss of *Pycard*^{-/-}, *Nlrp3*^{-/-}, and *Casp1*^{-/-} mice after DSS challenge. (E) Clinical parameters (weight loss, stool consistency, and bleeding) of indicated mice. These data are the averages of each clinical score collected throughout the recurring colitis model. (F) Colon length of indicated mice. (G) Colon histopathology scores reflecting the severity of inflammation, epithelial defects, crypt atrophy, and area affected in hematoxylin and eosin-stained sections through the mid and distal colon. The individual scores are shown in Fig. S2 and summed to generate a HAI. Colon length and histopathology were assessed in the *Casp1*^{-/-} animals on day 40, whereas these two parameters were assessed on day 57 in the other genotypes tested. Data shown are representative of three independent experiments and depict the mean ± SEM. Error bars have been omitted from the weight loss data for clarity of presentation. The symbols # and § indicate P < 0.05 and P < 0.01, respectively, between the mock- and DSS-treated WT; * indicates P < 0.05 between the DSS-treated gene-deficient strains and WT. WT mock, n = 5; WT, n = 5; *Pycard*^{-/-}, n = 3; *Casp1*^{-/-}, n = 4; *Nlrp3*^{-/-}, n = 3.

Casp1^{-/-} and *Pycard*^{-/-} mice demonstrate significantly increased clinical scores associated with enhanced gastrointestinal disease (Fig. 3 E). These clinical data suggest that PYCARD and caspase-1 are necessary for mouse survival and serve a protective role during inflammation-driven colon tumorigenesis. The rapid progression to a moribund state observed in the *Pycard*^{-/-} and *Casp1*^{-/-} mice upon AOM/DSS treatment suggests an increased pathological condition. In vivo tumorigenesis was evaluated by a gastroenterologist during week 6 of the AOM/DSS model in WT, *Pycard*^{-/-}, and *Casp1*^{-/-} mice via high-resolution endoscopy. All AOM/DSS-challenged animals demonstrated increased colon inflammation compared with mock-treated mice. Increased numbers of polypoid masses were identified in the colons of *Casp1*^{-/-} and *Pycard*^{-/-} mice (Fig. 3 F). Histopathological analysis revealed

that many of these masses were adenocarcinomas. All animals challenged with AOM/DSS also demonstrated a significant increase in colon histopathology (Fig. 3 G) with *Pycard*^{-/-} and *Casp1*^{-/-} mice exhibiting a significant increase in HAI compared with similarly treated WT animals. In the CAC model, the composite HAI is calculated as described for colitis alone, but also includes assessments of mid and distal colon hyperplasia and dysplasia (Meira et al., 2008). The scores of the individual HAI components are shown in Fig. S2. Increased inflammation, epithelial defects, disease area, and crypt atrophy was observed in the mid and distal colons from both *Pycard*^{-/-} and *Casp1*^{-/-} mice (Fig. S2, A–D). Significantly increased distal colon hyperplasia and dysplasia were observed in *Pycard*^{-/-} and *Casp1*^{-/-} mice compared with similarly treated WT animals (Fig. S2, E–F). *Pycard*^{-/-} and *Casp1*^{-/-} mice also show an increase in mid-colon hyperplasia and dysplasia compared with WT controls, but this increase was not statistically significant. These data demonstrate that the inflammasome components, PYCARD and caspase-1, function to attenuate inflammation and hyperplasia/dysplasia in the inflammation-driven colon tumorigenesis model.

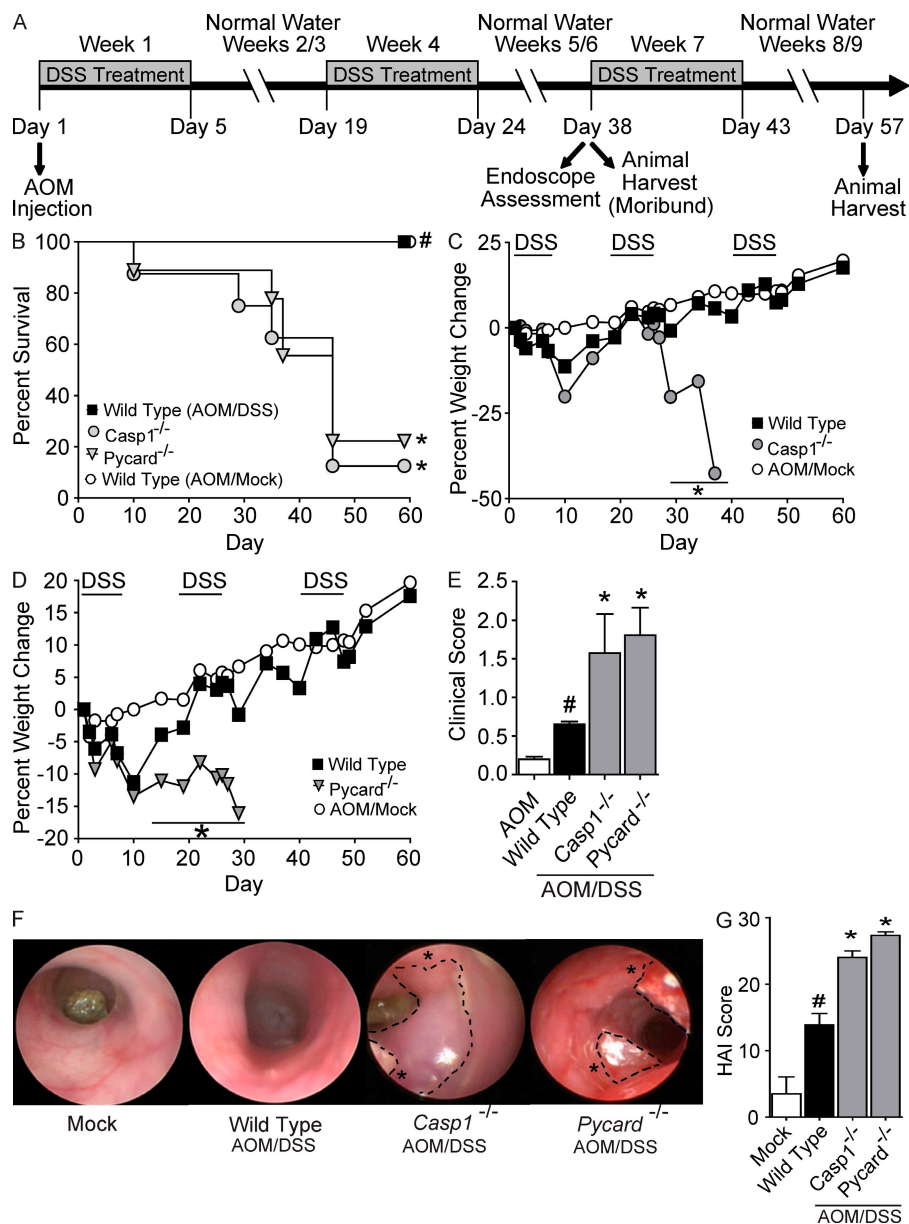


Figure 3. *Casp1*^{-/-} and *Pycard*^{-/-} mice are highly susceptible to inflammation-driven colon tumorigenesis. (A) Schematic of the four stage model of inflammation-driven tumor progression using the chemical carcinogen AOM and DSS. (B) Kaplan-Meier plot of WT, *Casp1*^{-/-}, and *Pycard*^{-/-} mouse survival. (C and D) Weight loss after AOM+DSS challenge. (E) Clinical parameters associated with increased gastrointestinal disease. (F) Inflammation and tumors revealed by in vivo high resolution endoscopy of during week 6 of the recurring colitis-driven tumor model. Asterisks indicate large tumors throughout the distal colons. (G) Colon histopathology scores reveal the severity of inflammation, epithelial defects, crypt atrophy, dysplasia, hyperplasia, and area affected in hematoxylin and eosin-stained sections through the mid and distal colon shown, as in Fig. S3. These scores were summed together to generate a HAI. Data shown are representative of three independent experiments and depict the mean \pm SEM. Error bars have been omitted from the weight loss data for clarity of presentation. The symbol # indicates $P < 0.05$ between the AOM/mock and AOM/DSS-treated WT; * indicates $P < 0.05$ between the gene-deficient strains and WT. For the survival study: WT AOM/mock, $n = 6$; *Casp1*^{-/-} $n = 8$; *Pycard*^{-/-} $n = 9$; WT $n = 9$. For all other datasets: WT AOM, $n = 3$; WT, $n = 9$; *Pycard*^{-/-}, $n = 6$; *Casp1*^{-/-}, $n = 3$.

IL-1 β and IL-18 levels are attenuated in colons isolated from *Pycard*^{-/-} and *Casp1*^{-/-} mice after the induction of CAC

PYCARD and caspase-1 are required for NLR- and absence in melanoma 2 (AIM2)-dependent inflammasome processing of IL-1 β and IL-18. In addition, each is known to have inflammasome-independent activities in regulating distinct aspects of cell death (Miura et al., 1993; Masumoto et al., 1999). To measure proinflammatory cytokine levels in the colons, organ cultures were established from mice that had completed the recurring colitis tumorigenesis model. Organ culture supernatants were harvested after incubation for 24 h and IL-1 β , IL-18, and TNF levels were determined by ELISA. Treatment with AOM and DSS caused a significant increase in proinflammatory cytokine levels in the WT mice (Fig. 4). IL-1 β and IL-18 levels were significantly attenuated

in the organ cultures from *Pycard*^{-/-} and *Casp1*^{-/-} animals (Fig. 4, A–B). This is consistent with the roles of PYCARD and caspase-1 in inflammasome processing of IL-1 β and IL-18. We also observed a decrease in TNF levels in the *Pycard*^{-/-} mice compared with WT (Fig. 4 C). This reduction in TNF is likely caused by an inflammasome-independent role for PYCARD in the regulation of TNF (Taxman et al., 2006). These data confirm that PYCARD and caspase-1 are required for the production of IL-1 β and IL-18 in the inflammation-driven colon tumorigenesis model. The increased inflammation and tumor burden observed in the *Pycard*^{-/-} and *Casp1*^{-/-} animals is correlated with a measurable loss of function of these two genes.

NLRP3 attenuates the development of gastrointestinal disease in CAC

PYCARD and caspase-1 are both required for the proper functioning of the majority of characterized NLR inflammasomes. If the phenotypes that we have described for the *Pycard*^{-/-} and *Casp1*^{-/-} mice are NLR dependent, we would predict that loss of a specific NLR would recapitulate

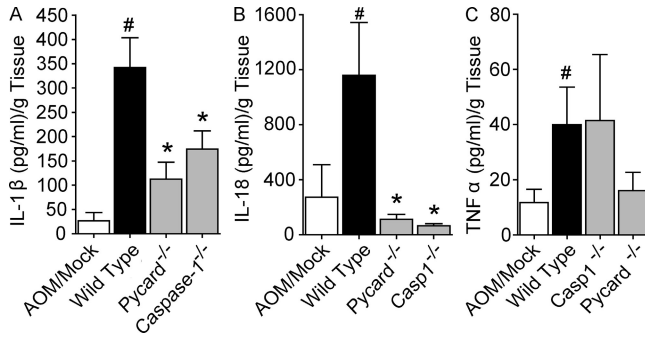


Figure 4. Reduced IL-1 β and IL-18 production in colons isolated from *Pycard* and caspase-1 deficient mice. Colons isolated from the indicated AOM+DSS-challenged mice were cultured overnight and IL-1 β (A), IL-18 (B), and TNF (C) in the supernatants was measured by ELISA. Data shown are representative of at least three independent experiments and depict the mean \pm SEM. The symbol # indicates $P < 0.05$ between the AOM/mock and AOM/DSS-treated WT; * indicates $P < 0.05$ between the gene-deficient strains and WT. AOM/mock, $n = 3$; WT, $n = 6$; *Pycard*^{-/-}, $n = 3$; *Casp1*^{-/-}, $n = 3$.

the observed phenotypes. NLRP3 can form an inflammatory complex with PYCARD and caspase-1 in response to a diverse range of environmental stressors and DAMPs (Martinon et al., 2006; Sutterwala et al., 2006; Eisenbarth et al., 2008; Li et al., 2008). Common variants in the *NLRP3* regulatory region have been shown to alter colonic *NLRP3* expression, IL-1 production and are associated with increased susceptibility to Crohn's disease (Villani et al., 2009). In addition to NLRP3, other NLRs, such as NLRC4, can form NLRP3-independent inflammasome in response to specific stimuli, such as flagellin (Mariathasan et al., 2004).

To determine the role of a specific NLR inflammasome, mice lacking either NLRP3 or NLRC4 were assessed in the inflammation-driven colon tumorigenesis model (Fig. 5 A). Unlike the survival phenotypes observed in the *Pycard*^{-/-} and *Casp1*^{-/-} mice, *Nlrp3*^{-/-} or *Nlrc4*^{-/-} animals did not progress to a moribund state requiring euthanasia (Fig. 5, B and C). *Nlrp3*^{-/-} mice exhibited a significant weight loss (Fig. 5 B) but the loss was attenuated compared with *Pycard*^{-/-} and *Casp1*^{-/-} animals shown earlier. Increased weight loss was also observed in *Nlrc4*^{-/-} mice after the final treatment of DSS (Fig. 5 C). However, the change was highly variable and was not a statistically significant difference compared with similarly treated WT animals. Consistent with the weight loss phenotype, *Nlrp3*^{-/-} mice demonstrate a significant increase in clinical scores associated with gastrointestinal disease compared with WT and *Nlrc4*^{-/-} animals (Fig. 5 D). They also exhibited significantly truncated colons compared with WT controls (Fig. 5 E). Gross morphological differences including extensive truncation, wall thickening, and hemorrhaging were also observed in the majority of colons harvested from *Nlrp3*^{-/-} mice compared with WT controls (Fig. 5 F). These data indicate that *Nlrp3*, but not *Nlrc4*, attenuates morbidity and clinical outcome associated with CAC, although the

effects are reduced compared with those observed for *Pycard*^{-/-} and *Casp1*^{-/-} mice.

NLRP3 deficiency enhances gastrointestinal tumorigenesis

To investigate the role of NLRP3 in tumor formation, we initially examined polyp formation via high-resolution endoscopy at the 6 wk time point. This corresponds with the time point associated with increased polypoid masses in the *Pycard*^{-/-} and *Casp1*^{-/-} mice (Fig. 3). All AOM/DSS-treated animals demonstrated increased colon inflammation compared with mock-treated mice; however, no tumors were observed via endoscopy in the *Nlrp3*^{-/-}, *Nlrc4*^{-/-}, or WT colons at this time point (Fig. 6 A). However, extensive ulcerated sections of colon and fibrinogen deposition were identified in *Nlrp3*^{-/-} mice (Fig. 6 A). These highly abnormal ulcerated sections of colon are indicative of precancerous lesions, thus leading us to examine if *Nlrp3*^{-/-} mice would develop increased tumorigenesis during later stages of the CAC model.

Upon completion of the CAC model (week 9), macroscopic colon polyps were detected in the majority of AOM/DSS-treated mice (Fig. 6 B). However, a dramatic increase in the mean number of polyps was observed in the colons of *Nlrp3*^{-/-} mice (4.5 ± 0.95) compared with those isolated from the WT (1 ± 0.45) or *Nlrc4*^{-/-} animals (0.57 ± 0.30 ; Fig. 6 B). In addition to greater frequencies, these polyps were also much larger in both maximal cross-sectional area and wet weight compared with the polyps isolated from WT mice (Fig. 6 C). Colon histopathology revealed a significant increase in the HAI score from all AOM/DSS-treated animals when compared with AOM/mock-treated WT mice. Increased HAI scores were observed for *Nlrp3*^{-/-} mice compared with WT and *Nlrc4*^{-/-} animals (Fig. 6 D). However, when compared with the HAI of similarly treated *Pycard*^{-/-} (27.33 ± 0.54) and *Casp1*^{-/-} mice (24.00 ± 1.00) shown earlier (Fig. 3 G), the HAI for the *Nlrp3*^{-/-} mice (19.00 ± 1.39) was significantly reduced (Fig. 6 D). These findings are consistent with the attenuated and slower disease progression observed in the *Nlrp3*^{-/-} animals compared with the rapid disease progression found in *Pycard*^{-/-} and *Casp1*^{-/-} mice. As expected by the increase in polyp number, a significant increase in distal colon hyperplasia, dysplasia, and area involved with pathology was observed in the *Nlrp3*^{-/-} mice compared with similarly treated WT and *Nlrc4*^{-/-} animals (Figs. 6, E–G). In contrast to the findings for the *Pycard*^{-/-} and *Casp1*^{-/-} mice, inflammation and midcolon disease parameters were similar between the WT, *Nlrc4*^{-/-}, and *Nlrp3*^{-/-} animals (Fig. S3). These data indicate that *Nlrp3*^{-/-} mice exhibit an attenuated disease when compared with *Pycard*^{-/-} and *Casp1*^{-/-} mice; however, the composite data support the hypothesis that this gene product negatively regulates tumorigenesis in the CAC model.

NLRP3 mediates gastrointestinal disease through hematopoietic-derived cells

We next sought to establish the relevant cell compartment of the host that is responsible for the increased susceptibility to

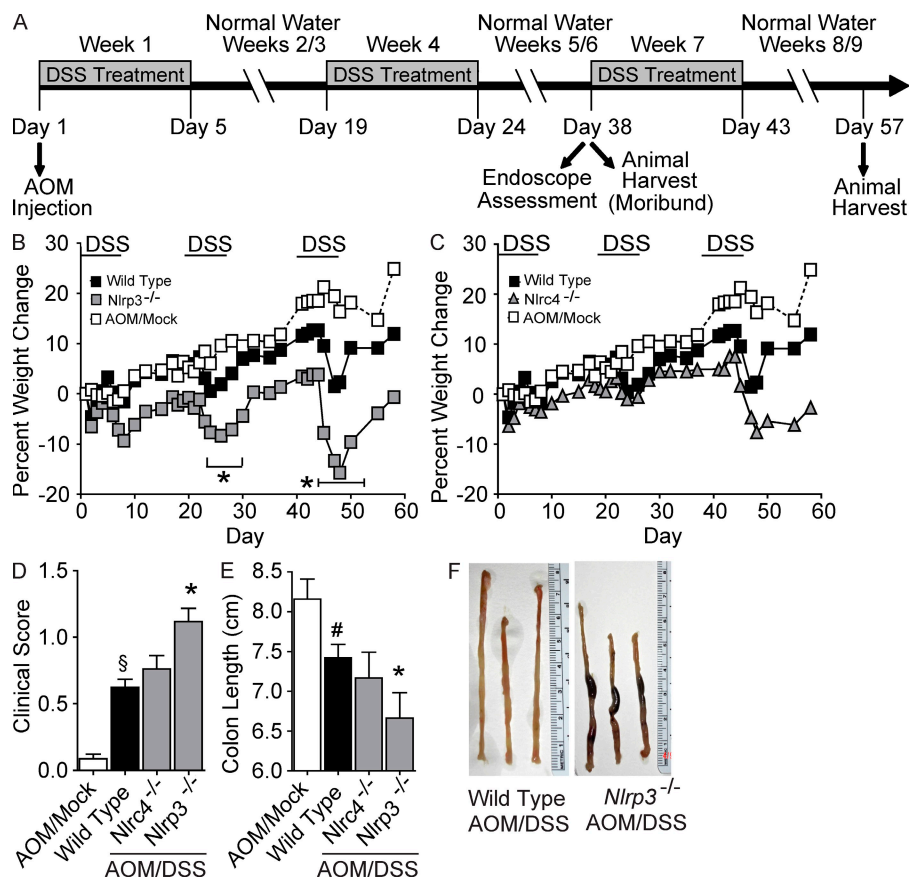


Figure 5. Loss of *Nlrp3* results in augmented features of ulcerative colitis in the inflammation-driven tumor model.

(A) Schematic of the CAC model using the chemical carcinogen AOM and DSS. (B and C) Weight loss measured throughout the colitis driven tumor progression model in WT, *Nlrp3*^{-/-}, and *Nlrp4*^{-/-} mice (difference observed during the final week of study in C is not statistically significant). (D) Clinical scores reflecting weight loss, loose stool consistency, and amounts of blood present in stool and rectum. (E) Colon length. (F) Gross morphology revealing areas of excessive wall thickening and hemorrhage. Data shown are representative of 3 independent experiments and depict the mean ± SEM. Error bars have been omitted from the weight loss data for clarity of presentation. The symbols # and \$ indicate $P < 0.05$ and $P < 0.01$, respectively, between the AOM/mock and AOM/DSS-treated WT; * indicates $P < 0.05$ between the *Nlrp3*^{-/-} and WT mice. WT, $n = 15$; *Nlrp3*^{-/-}, $n = 12$; *Nlrp4*^{-/-}, $n = 4$; WT AOM/mock, $n = 3$.

CAC in the *Nlrp3*^{-/-} mice. The intestinal epithelial cells and stroma play a critical role in gastrointestinal biology by providing the physical separation between the gut microflora and the cells of the mucosal immune system. Gut microflora is believed to provide the carcinogenic metabolism of hydroxylated AOM that enables its colonotropic mutagenicity within the intestinal epithelial cells in the AOM model (Reddy et al., 1974). Additional data suggest that hematopoietic cells including macrophages and other myeloid-derived cells also play important but divergent roles in regulating colonic tumor initiation, growth, and metastasis (Biswas et al., 2008).

To determine the cellular compartment responsible for the phenotype observed in the *Nlrp3*^{-/-} mice, we generated chimeric animals by adoptive bone marrow transplantation, and then subjected the mice to the AOM/DSS colon tumorigenesis model (Fig. 7 A). As seen in Fig. 7 B, WT-irradiated recipients that received WT bone marrow did not demonstrate substantial weight loss during the recurring colitis model, whereas *Nlrp3*^{-/-} recipients of *Nlrp3*^{-/-} bone marrow experienced a significant decrease in weight, indicating that the bone marrow chimerization procedure did not alter the more significant weight loss observed in the *Nlrp3*^{-/-} mice. However, the pattern of weight loss in bone marrow chimeras occurred during the first two rounds of DSS treatment rather than the latter two rounds, as observed with unirradiated animals (Fig. 5 B). These differences might be

attributed to the radiation and hematopoietic reconstitution process, nonetheless in both experimental designs, *Nlrp3*^{-/-} mice showed significantly more weight loss than WT. *Nlrp3*^{-/-} animals that received WT bone marrow demonstrate significantly less weight loss compared with *Nlrp3*^{-/-} mice and WT animals that received *Nlrp3*^{-/-} bone marrow. This indicates that the source of the hematopoietic compartment determines the outcome of weight loss. Consistent with the weight loss data, animals receiving *Nlrp3*^{-/-} bone marrow demonstrated significantly increased clinical scores compared with mice receiving WT bone marrow (Fig. 7 C). Recipients of *Nlrp3*^{-/-} bone marrow also demonstrate truncated colons compared with animals transplanted with WT bone marrow (Fig. 7 D). These clinical data suggest that the phenotype observed in the *Nlrp3*^{-/-} mice is associated with hematopoietic-derived cells rather than the intestinal epithelial cells, tumor-derived cells, or stroma.

To extend the clinical findings, tumorigenesis, and inflammation was characterized in the chimeric mice harvested 2 wk after the completion of the third round of DSS in the CAC model. Mice receiving *Nlrp3*^{-/-} but not WT bone marrow also demonstrated significantly increased colonic lesions (Fig. 7 E), including increased distal colon inflammation, hyperplasia, dysplasia, and area associated with disease (Fig. S4, A–F). Similar to *Nlrp3*^{-/-} animals, recipients of *Nlrp3*^{-/-} bone marrow exhibited an increase in the number of colonic macroscopic polyps (Fig. 7 F). Together, the clinical and histopathology data indicate that NLRP3 regulates gastrointestinal tumorigenesis through hematopoietic-derived cells in models of CAC.

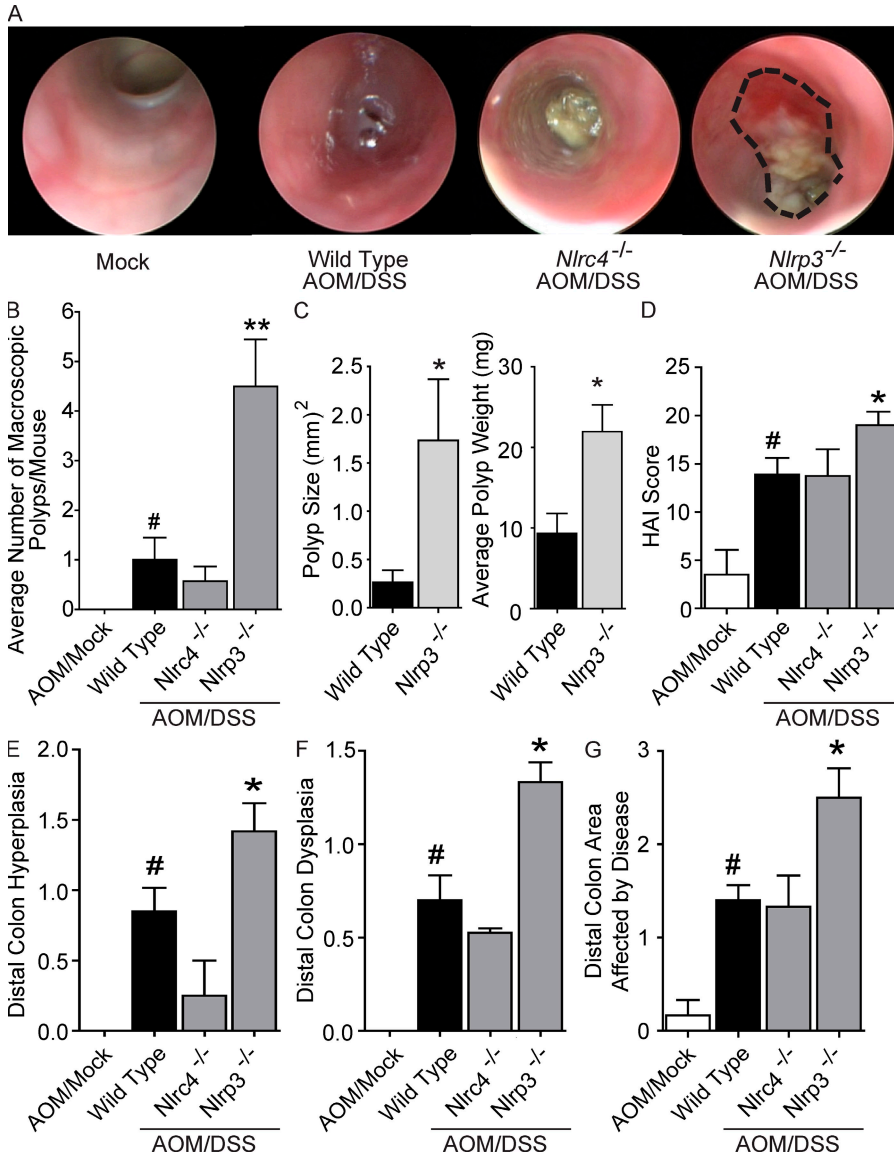


Figure 6. NLRP3 mediates gastrointestinal tumorigenesis in the CAC model.

(A) Endoscopic analysis of mice during week 6 of the recurring CAC model. (B) Macroscopic polyps were quantified in indicated mice. (C) Size and weight of representative macroscopic polyps from indicated mice. (D) Composite HAI scores. (E–G) Distal colon hyperplasia (E), dysplasia (F), and area involved with disease (G). Data are representative of three independent experiments. The symbol # indicates $P < 0.05$ between the AOM/mock and AOM/DSS-treated WT; * and ** indicate $P < 0.05$ and $P < 0.01$, respectively, between the *Nlrp3*^{-/-} and WT mice. WT AOM, $n = 3$; WT, $n = 10$; *Nlrp3*^{-/-}, $n = 3$; *Nlrp3*^{-/-}, $n = 6$.

is associated with reduced inflammatory function at the tumor site.

Our data show that the NLR inflammasome components PYCARD, caspase-1, and NLRP3 might function as inflammation and tumor suppressors in the inflammation-driven colon tumorigenesis model. *Pycard*^{-/-} and *Casp1*^{-/-} mice have significantly attenuated NLR inflammasome activity. Despite reduced levels of proinflammatory IL-1 β and IL-18 within the site of polyp formation, both sets of genetically altered mice developed increased areas of local inflammation and enhanced dysplasia and hyperplasia. It should be noted that our data present a correlative link between the dysregulation of IL-1 β and IL-18 and the development of gastrointestinal

DISCUSSION

A current dogma in cancer immunology suggests that inflammation functions as a tumor promoter. Components of the inflammasome function to process pro-IL-1 β and -IL-18 into mature cytokines, thus an initial hypothesis centered on the concept that increased inflammation caused by inflammasome formation creates a local environment that is favorable for tumorigenesis. This hypothesis predicts reduced inflammation and attenuated tumorigenesis in mice lacking NLR inflammasome components. However, the data presented throughout this study, have led us to propose a protective role for the inflammasome during chronic colitis and colitis-associated colon cancer. These results parallel other findings in the literature that suggest that other innate immune sensors, such as MyD88, can serve as a protective and homeostatic factor in the intestine (Araki et al., 2005). In our work, we also find that deficiencies in diverse inflammasome components can lead to enhanced colitis, as well as CAC that

is directly related to the increase in colitis and colitis-associated tumorigenesis. One possible explanation of enhanced tumorigenesis observed in the *Pycard*^{-/-} and *Casp1*^{-/-} mice can be attributed to their previously defined roles associated with programmed cell death. Pycard was originally found to increase the susceptibility of leukemia cell lines to apoptotic stimuli associated with anticancer drugs (Masumoto et al., 1999). Likewise, caspase-1-mediated cell death has been shown to be suppressed by BCL2 overexpression (Miura et al., 1993). An alternative explanation is that the increased susceptibility of these mice to CAC may be caused by the loss of downstream signaling mediated by the respective receptors for either IL-1 β or IL-18. For example, MyD88 is involved in IL-1 and IL-18 receptor signaling. Other investigators have previously shown that MyD88 and TLR signaling can maintain homeostasis and protect the intestine upon DSS-induced or bacteria-induced colitis, partly by the recognition

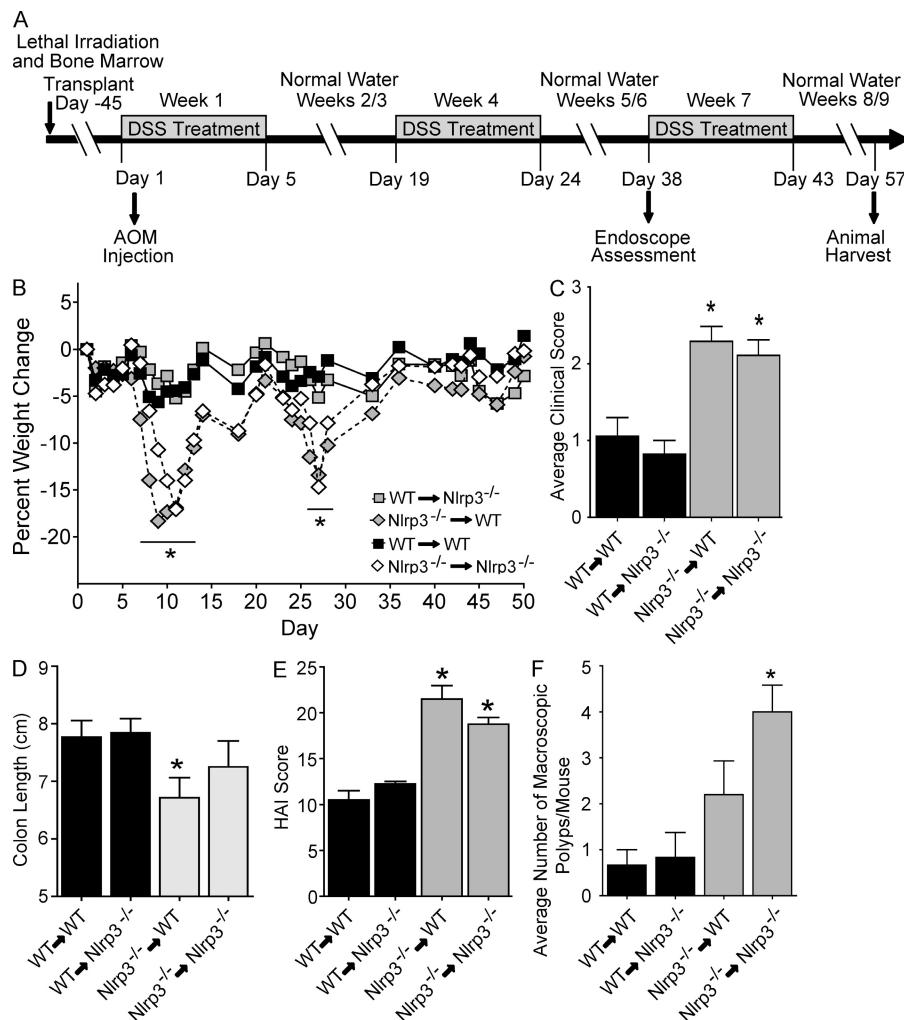


Figure 7. Mice receiving bone marrow from *Nlrp3*^{-/-} animals develop enhanced gastrointestinal disease. (A) Schematic of the four stage model of inflammation-driven tumor progression using the chemical carcinogen AOM in bone marrow chimeric mice. (B) Weight change of indicated BM chimeras. (C) Composite clinical scores reflecting weight loss, loose stool consistency, and blood in the stool and rectum. (D) Colon length. (E) Composite HAI scores. (F) Quantification of macroscopic polyps. Data depict the mean \pm SEM and are representative of three independent experiments. The symbol * indicates $P < 0.05$ in a comparison of the WT \rightarrow WT control to the other three groups. WT \rightarrow Nlrp3^{-/-}, $n = 7$; Nlrp3^{-/-} \rightarrow WT, $n = 7$; WT \rightarrow WT, $n = 3$; Nlrp3^{-/-} \rightarrow Nlrp3^{-/-}, $n = 3$.

of commensal normal flora in the intestine (Rakoff-Nahoum et al., 2004; Araki et al., 2005; Fukata et al., 2005). However, in several cases of spontaneous or chemical-induced colitis, MyD88 has been found to act as a tumor promoter. In an AOM-exposed, *Il10*^{-/-} mouse model, MyD88 is required for the development of neoplastic lesions (Uronis et al., 2009). In a spontaneous tumor model caused by a mutation in the adenomatous polyposis coli gene, MyD88 exacerbated intestinal polyp development partly by reducing apoptosis (Rakoff-Nahoum and Medzhitov, 2007). In contrast to these findings, *T-bet*^{-/-}, *RAG2*^{-/-} mice that exhibited spontaneous UC that progressed to adenocarcinoma did not involve MyD88 (Garrett et al., 2009). These findings suggest that the role of MyD88 in tumorigenesis is complex, and likely varies with genetic variations, tissue/cellular involvement, and timing of carcinogenic insult.

Our findings are also unexpected based on previously published findings on the role of caspase-1 in models of colitis (Siegmond et al., 2001; Bauer et al., 2007). Several explanations are possible to explain the observed differences between the various studies. For example, mouse background and gender can have dramatic effects in the DSS model of

colitis. Likewise, colitis models can be significantly influenced by several variables that are unique to each specific institution including: differences in the gastrointestinal microflora between the various animal facilities, differences in the type of water (deionized, autoclaved, or tap) used to administer the DSS, and differences in the concentration and duration of administration of the DSS treatments. We have attempted to minimize these variables using both physical mechanisms (i.e., housing all of our animals in the same building/same room under SPF conditions, making fresh DSS each day, using the same type of water for all experiments, and using only male mice) and using a standardized, published protocol for the DSS and AOM/DSS models (Neufert et al., 2007).

Our data show that the inflammasome component NLRP3 also plays a role in reducing acute colitis and colitis-associated colon cancer. However, the modulating effect of NLRP3 on colon cancer is both attenuated and delayed during CAC development compared with the roles played by PYCARD and caspase-1. This suggests that other NLR or non-NLR inflammasome components could contribute to the development of CAC. Although NLRP3 and NLRC4 are the most extensively characterized NLRs that mediate inflammasome formation, NLRC4 does not have a significant role in CAC. We chose to assess NLRC4 because of its well characterized role in forming an inflammasome in response to flagellated gastrointestinal pathogens such as *Salmonella* and *Shigella* (Lamkanfi and Dixit, 2009). In addition to the NLRs, the recently described AIM2 gene is of particular interest because it is reduced or absent in several cancers and its restoration caused cell cycle arrest in colon cancer cell types (Patsos et al., 2010). AIM2 has been shown to form

an NLRP3-independent inflammasome with Pycard and caspase-1 in response to cytoplasmic DNA, which then processes IL-1 β and IL-18 (Bürckstümmer et al., 2009; Fernandes-Alnemri et al., 2009; Hornung et al., 2009). It will be interesting to test the role played by inflammasome components such as AIM2 when mice lacking this gene become available.

Based on the mechanism of action for DSS (initiating a wound-healing response in the colonic epithelial layer), it is our belief that the phenotypes we are observing in the *Nlrp3*^{-/-} mice are likely caused by an indirect mechanism. We attempted to directly activate the inflammasome with DSS in bone marrow-derived macrophages, and our initial analysis suggests that DSS does not directly induce the production of IL-1 β (unpublished data). However, damage to the colonic epithelial cell layer in the colon initiates the release of various DAMP signals, and DAMPs have the potential to activate the NLRP3 inflammasome. Thus, it is possible that a failure of the hematopoietic cells to recognize and effectively cope with these indirect signals results in the eventual development of increased CAC.

Our data suggest that NLRP3 regulates tumorigenesis through the hematopoietic/myeloid compartment. This finding is consistent with the known biology of NLRP3 because the vast majority of NLRP3's function can be attributed to its presence in myeloid-derived cells, specifically monocytes/macrophages. Tumor-associated myeloid-derived cells demonstrate a great deal of flexibility throughout the course of tumor progression. During conditions of chronic inflammation, such as IBD, macrophages can initiate tumorigenesis through the release of proinflammatory mediators and other factors that promote neoplastic transformation. Once a tumor becomes established, macrophages and myeloid-derived cells create a local environment which can be immunosuppressive and is thus favorable for tumor growth, angiogenesis, and metastasis. However, monocytes/macrophages are also involved in the antitumor response of the host by functioning as cytotoxic effector cells, inducing reactive oxygen species and producing cytokines such as IL-12, which has anti-proliferative, antiangiogenic, and cytotoxic effects through the subsequent generation of IFN- γ (Nardin and Abastado, 2008). In the gut, myeloid-derived cells also act as tumor-associated antigen-presenting cells and are responsible for efficient phagocytosis and removal of apoptotic/tumorigenic cells (Zitvogel et al., 2006).

In summary, the two-hit model of inflammasome formation posits that IL-1 β /IL-18 processing requires a first hit that is mediated by signals such as TLR and MyD88 resulting in increased pro-IL-1 β /IL-18 transcription and a second hit that initiates the posttranslational processing of caspase-1, IL-1 β , and IL-18 proteins by the inflammasome components. The findings of this study suggest that both signals, emanating from two distinct classes of innate immune sensors, serve to attenuate colitis and CAC. Further understanding of the specific roles of the NLRs and inflammasome-associated adaptor

proteins in mediating the host innate immune response to cancer will allow the generation of improved cancer therapeutics. As a cautionary note, our findings also suggest that when therapies targeting individual inflammasome components become available, their unintended effects on CAC should be closely monitored.

MATERIALS AND METHODS

Experimental animals. All studies were approved by the Institutional Care and Use Committee of The University of North Carolina at Chapel Hill and were conducted in accordance with the IACUC guidelines and the National Institutes of Health Guide for the Care and Use of Laboratory Animals. The generation of mice lacking functional *Nlrp3*, *Nlr4*, *Pycard*, and caspase-1 (*Casp1*) has been previously described (R. Flavell, Yale University, New Haven, CT; V. Dixit, Genentech, Inc., San Francisco, CA; F. Sutterwala, University of Iowa, Iowa City, IA; Adachi et al., 1998; Mariathasan et al., 2004; Sutterwala et al., 2006). All experiments were conducted with age-matched male mice, and all mice were backcrossed at least nine generations onto the C57BL/6. Mice were housed under SPF conditions and provided 5010 chow (LabDiet) and water ad libitum.

Induction of colitis and inflammation-driven tumor progression.

To assess the induction of acute colitis, all mice were subjected to one cycle of 5% DSS (MP Biomedicals) exposure as illustrated in Fig. 1 A. To assess the induction of recurring UC, mice were exposed to 3 cycles of 2.5% DSS as illustrated in Fig. 2 A (without the addition of AOM; Neufert et al., 2007). Mice were sacrificed and inflammation assessments made at specific time points throughout the course of the challenge. To evaluate tumorigenesis, mice received 1 i.p. injection (10 mg/kg body weight) of AOM (Sigma-Aldrich) followed by 3 cycles of DSS treatments (2.5%; Fig. 3 A). Mice were sacrificed and tumor assessments made 10 wk after AOM injection or when moribund.

Body weight, the presence of rectal bleeding, and stool consistency were scored and averaged to generate a semiquantitative clinical score as previously described (Siegmund et al., 2001). In brief, body weight and stool consistency were assessed at least 5 d per week throughout the course of the DSS exposure. Rectal bleeding was assessed 1 d and 4 d after each DSS treatment by sampling for the presence of blood in the stool using a Hemoccult Immunochemical Fecal Occult Blood Test (Beckman Coulter). In addition to the composite clinical score, colon lengths were measured for each animal at the completion of each study.

Endoscopic tumor investigation. To evaluate tumor growth and progression in vivo, mice were anesthetized with isoflurane (Minrad, Inc.) and monitored by miniendoscopy, as previously described (Uronis et al., 2007). In brief, endoscopy was performed during week 6 of the UC and CAC models using a "Coloview system" (Karl Storz Veterinary Endoscope) and each session was digitally recorded. If fecal matter obstructed visualization, colons were flushed with 1X PBS. After air inflation, the colonoscopy allowed for the real-time evaluation of ~3–4 cm of colon from the anal verge to the splenic flexure.

Macroscopic polyp analysis and histopathology. Upon harvest, the entire colon was removed (rectum to cecum), flushed to remove fecal matter, and opened longitudinally. Macroscopic polyps were identified by analysis under a dissecting microscope (10 \times magnification) by a trained investigator, and the number and size of polyps were assessed in their maximum dimension.

For histopathology, the entire colon was removed, flushed with PBS, opened longitudinally, swiss rolled, and fixed in 10% buffered formalin. Subsequently, paraffin embedded samples were sectioned at 5 μ m, stained with hematoxylin and eosin and evaluated by a trained veterinary pathologist, as previously described (Meira et al., 2008). In brief, sections were

scored blindly for inflammation, epithelial defects, crypt atrophy, hyperplasia, dysplasia/neoplasia, and area affected by dysplasia. Inflammation was determined based on the number and extent of leukocyte infiltration. Epithelial defects were determined based on the severity of damage to the epithelial cell layer. Crypt atrophy was scored based on visual estimates of the percent of atrophy in the crypts of the most affected areas of colon. Hyperplasia and dysplasia were scored based on the severity of the cellular changes induced by disease and ranged from mild atypia to intramucosal carcinoma.

Colon organ culture and proinflammatory mediator assessments.

To assess the local levels of IL-1 β , IL-18, and TNF, we generated organ cultures from control, DSS, and AOM/DSS challenged mice as previously described (Greten et al., 2004). In brief, the colons were removed and cut open longitudinally. These strips were washed with PBS containing penicillin/streptomycin, the distalmost 3 cm were isolated and further cut into 1-cm² sections, and the wet weight of each was recorded. Colon sections were covered with RPMI media, including penicillin/streptomycin, and incubated overnight. Cell-free supernatants were harvested and assayed via ELISA for IL-1 β , IL-18, and TNF.

Generation of chimeric mice by bone marrow reconstitution.

To evaluate the hematopoietic cell contribution to the initiation and progression of tumorigenesis, chimeric mice were generated using bone marrow transplantation following standard protocols. In brief, recipient mice were lethally irradiated (single dose of γ -irradiation, 950 rad) and 12 h later the mice received 5×10^6 bone marrow cells flushed from the femurs and tibias of WT and *Nlrp3*^{-/-} mice. Bone marrow was harvested and prepared following standard procedures. The bone marrow reconstitution was performed reciprocally, resulting in the generation of four groups of experimental mice. The surviving mice were subjected to the 4-stage AOM/DSS model, 6 wk after transplantation.

Statistical analysis. Data are presented as the mean \pm SEM. Analysis of variance followed by either Tukey-Kramer HSD or Newman-Keuls Post Test for multiple comparisons was performed on complex datasets for both individual experiments and composite data. Statistical significance for single data points were assessed by the Student's two-tailed *t* test. Survival curves were generated using the product limit method of Kaplan and Meier, and comparisons were made using the log-rank test. In all cases, a *P* value of >0.05 was considered statistically significant.

Online supplemental material. In Fig. S1, *Pycard*^{-/-} mice demonstrate increased mid and distal colon histopathology in the recurring ulcerative colitis model. In Fig. S2, *Casp1*^{-/-}, and *Pycard*^{-/-} mice demonstrate increased mid and distal colon histopathology in the CAC model. Fig. S3 shows increased gastrointestinal disease was localized to the distal colon in the *Nlrp3*^{-/-} mice. Fig. S4 shows increased histopathology in mice receiving *Nlrp3*^{-/-} bone marrow. Online supplemental material is available at <http://www.jem.org/cgi/content/full/jem.20100050/DC1>.

The authors thank the Center for Gastrointestinal Biology and Disease for providing core and technical support (P30DK34987). We also thank Drs. Richard Flavell, Vishva M. Dixit, Fayyaz Sutterwala, and Millenium Pharmaceuticals for supplying the *Nlrp3*^{-/-}, *Pycard*^{-/-}, *Nlr4*^{-/-}, and *Casp1*^{-/-} mice. In addition, we would like to acknowledge Dr. Marcus Mühlbauer, Dr. Justin Wilson, and Dr. Hendrick vanDeventer for technical assistance.

This work is supported by U19-AI077437-01 and UNC-UCRF (J.P.-Y. Ting); T32HD046369 (E.K. Holl); and F32AI082895, P30DK34987 (UNC CGIBD), T32CA009156, T32AR007416, and the American Cancer Society (PF-10-053-01-LIB; I.C. Allen).

The authors have no conflicting financial interests.

Submitted: 7 January 2010

Accepted: 24 March 2010

REFERENCES

- Adachi, O., T. Kawai, K. Takeda, M. Matsumoto, H. Tsutsui, M. Sakagami, K. Nakanishi, and S. Akira. 1998. Targeted disruption of the MyD88 gene results in loss of IL-1- and IL-18-mediated function. *Immunity*. 9:143–150. doi:10.1016/S1074-7613(00)80596-8
- Agostini, L., F. Martinon, K. Burns, M.F. McDermott, P.N. Hawkins, and J. Tschopp. 2004. NALP3 forms an IL-1 β -processing inflammasome with increased activity in Muckle-Wells autoinflammatory disorder. *Immunity*. 20:319–325. doi:10.1016/S1074-7613(04)00046-9
- Akira, S., S. Uematsu, and O. Takeuchi. 2006. Pathogen recognition and innate immunity. *Cell*. 124:783–801. doi:10.1016/j.cell.2006.02.015
- Araki, A., T. Kanai, T. Ishikura, S. Makita, K. Uraushihara, R. Iiyama, T. Totsuka, K. Takeda, S. Akira, and M. Watanabe. 2005. MyD88-deficient mice develop severe intestinal inflammation in dextran sodium sulfate colitis. *J. Gastroenterol.* 40:16–23. doi:10.1007/s00535-004-1492-9
- Barber, M.D., J.J. Powell, S.F. Lynch, K.C. Fearon, and J.A. Ross. 2000. A polymorphism of the interleukin-1 beta gene influences survival in pancreatic cancer. *Br. J. Cancer*. 83:1443–1447. doi:10.1054/bjoc.2000.1479
- Bauer, C., F. Lohrer, M. Dauer, C. Mayer, H.A. Lehr, M. Schönharting, R. Hallwachs, S. Endres, and A. Egler. 2007. The ICE inhibitor pralnacasan prevents DSS-induced colitis in C57BL/6 mice and suppresses IP-10 mRNA but not TNF-alpha mRNA expression. *Dig. Dis. Sci.* 52:1642–1652. doi:10.1007/s10620-007-9802-8
- Bioque, G., J.B. Crusius, I. Koutroubakis, G. Bouma, P.J. Kostense, S.G. Meuwissen, and A.S. Peña. 1995. Allelic polymorphism in IL-1 beta and IL-1 receptor antagonist (IL-1RA) genes in inflammatory bowel disease. *Clin. Exp. Immunol.* 102:379–383.
- Biswas, S.K., A. Sica, and C.E. Lewis. 2008. Plasticity of macrophage function during tumor progression: regulation by distinct molecular mechanisms. *J. Immunol.* 180:2011–2017.
- Bürckstümmer, T., C. Baumann, S. Blüml, E. Dixit, G. Dürnberger, H. Jahn, M. Planyavsky, M. Bilban, J. Colinge, K.L. Bennett, and G. Superti-Furga. 2009. An orthogonal proteomic-genomic screen identifies AIM2 as a cytoplasmic DNA sensor for the inflammasome. *Nat. Immunol.* 10:266–272. doi:10.1038/ni.1702
- Casini-Raggi, V., L. Kam, Y.J. Chong, C. Fiochi, T.T. Pizarro, and F. Cominelli. 1995. Mucosal imbalance of IL-1 and IL-1 receptor antagonist in inflammatory bowel disease. A novel mechanism of chronic intestinal inflammation. *J. Immunol.* 154:2434–2440.
- Cassel, S.L., S. Joly, and F.S. Sutterwala. 2009. The NLRP3 inflammasome: a sensor of immune danger signals. *Semin. Immunol.* 21:194–198. doi:10.1016/j.smim.2009.05.002
- Coussens, L.M., and Z. Werb. 2002. Inflammation and cancer. *Nature*. 420:860–867. doi:10.1038/nature01322
- Eaden, J.A., K.R. Abrams, and J.F. Mayberry. 2001. The risk of colorectal cancer in ulcerative colitis: a meta-analysis. *Gut*. 48:526–535. doi:10.1136/gut.48.4.526
- Eisenbarth, S.C., O.R. Colegio, W. O'Connor, F.S. Sutterwala, and R.A. Flavell. 2008. Crucial role for the Nalp3 inflammasome in the immunostimulatory properties of aluminium adjuvants. *Nature*. 453:1122–1126. doi:10.1038/nature06939
- El-Omar, E.M., M. Carrington, W.H. Chow, K.E. McColl, J.H. Bream, H.A. Young, J. Herrera, J. Lissowska, C.C. Yuan, N. Rothman, et al. 2001. The role of interleukin-1 polymorphisms in the pathogenesis of gastric cancer. *Nature*. 412:99. doi:10.1038/35083631
- Fernandes-Alnemri, T., J.W. Yu, P. Datta, J. Wu, and E.S. Alnemri. 2009. AIM2 activates the inflammasome and cell death in response to cytoplasmic DNA. *Nature*. 458:509–513. doi:10.1038/nature07710
- Franchi, L., C. McDonald, T.D. Kanneganti, A. Amer, and G. Núñez. 2006. Nucleotide-binding oligomerization domain-like receptors: intracellular pattern recognition molecules for pathogen detection and host defense. *J. Immunol.* 177:3507–3513.
- Fukata, M., and M.T. Abreu. 2009. Pathogen recognition receptors, cancer and inflammation in the gut. *Curr. Opin. Pharmacol.* 9:680–687. doi:10.1016/j.coph.2009.09.006
- Fukata, M., K.S. Michelsen, R. Eri, L.S. Thomas, B. Hu, K. Lukasek, C.C. Nast, J. Lechago, R. Xu, Y. Naiki, et al. 2005. Toll-like receptor-4 is required for intestinal response to epithelial injury and limiting bacterial

- translocation in a murine model of acute colitis. *Am. J. Physiol. Gastrointest. Liver Physiol.* 288:G1055–G1065. doi:10.1152/ajpgi.00328.2004
- Garrett, W.S., S. Punit, C.A. Gallini, M. Michaud, D. Zhang, K.S. Sigrist, G.M. Lord, J.N. Glickman, and L.H. Glimcher. 2009. Colitis-associated colorectal cancer driven by T-bet deficiency in dendritic cells. *Cancer Cell.* 16:208–219. doi:10.1016/j.ccr.2009.07.015
- Greten, F.R., L. Eckmann, T.F. Greten, J.M. Park, Z.W. Li, L.J. Egan, M.F. Kagnoff, and M. Karin. 2004. IKKbeta links inflammation and tumorigenesis in a mouse model of colitis-associated cancer. *Cell.* 118:285–296. doi:10.1016/j.cell.2004.07.013
- Hornung, V., A. Ablasser, M. Charrel-Dennis, F. Bauernfeind, G. Horvath, D.R. Caffrey, E. Latz, and K.A. Fitzgerald. 2009. AIM2 recognizes cytosolic dsDNA and forms a caspase-1-activating inflammasome with ASC. *Nature.* 458:514–518. doi:10.1038/nature07725
- Lamkanfi, M., and V.M. Dixit. 2009. Inflammasomes: guardians of cytosolic sanctity. *Immunol. Rev.* 227:95–105. doi:10.1111/j.1600-065X.2008.00730.x
- Li, H., S.B. Willingham, J.P. Ting, and F. Re. 2008. Cutting edge: inflammasome activation by alum and alum's adjuvant effect are mediated by NLRP3. *J. Immunol.* 181:17–21.
- Mariathasan, S., K. Newton, D.M. Monack, D. Vucic, D.M. French, W.P. Lee, M. Roose-Girma, S. Erickson, and V.M. Dixit. 2004. Differential activation of the inflammasome by caspase-1 adaptors ASC and Ipaf. *Nature.* 430:213–218. doi:10.1038/nature02664
- Martino, F., V. Pétrilli, A. Mayor, A. Tardivel, and J. Tschopp. 2006. Gout-associated uric acid crystals activate the NALP3 inflammasome. *Nature.* 440:237–241. doi:10.1038/nature04516
- Masumoto, J., S. Taniguchi, K. Ayukawa, H. Sarvotham, T. Kishino, N. Niikawa, E. Hidaka, T. Katsuyama, T. Higuchi, and J. Sagara. 1999. ASC, a novel 22-kDa protein, aggregates during apoptosis of human promyelocytic leukemia HL-60 cells. *J. Biol. Chem.* 274:33835–33838. doi:10.1074/jbc.274.48.33835
- Meira, L.B., J.M. Bugni, S.L. Green, C.W. Lee, B. Pang, D. Borenshtein, B.H. Rickman, A.B. Rogers, C.A. Moroski-Erkul, J.L. McFaline, et al. 2008. DNA damage induced by chronic inflammation contributes to colon carcinogenesis in mice. *J. Clin. Invest.* 118:2516–2525.
- Miura, M., H. Zhu, R. Rotello, E.A. Hartwig, and J. Yuan. 1993. Induction of apoptosis in fibroblasts by IL-1 beta-converting enzyme, a mammalian homolog of the *C. elegans* cell death gene *ced-3*. *Cell.* 75:653–660. doi:10.1016/0092-8674(93)90486-A
- Nardin, A., and J.P. Abastado. 2008. Macrophages and cancer. *Front. Biosci.* 13:3494–3505. doi:10.2741/2944
- Neufert, C., C. Becker, and M.F. Neurath. 2007. An inducible mouse model of colon carcinogenesis for the analysis of sporadic and inflammation-driven tumor progression. *Nat. Protoc.* 2:1998–2004. doi:10.1038/nprot.2007.279
- Ogura, Y., D.K. Bonen, N. Inohara, D.L. Nicolae, F.F. Chen, R. Ramos, H. Britton, T. Moran, R. Karaliuskas, R.H. Duerr, et al. 2001. A frameshift mutation in NOD2 associated with susceptibility to Crohn's disease. *Nature.* 411:603–606. doi:10.1038/35079114
- Patsos, G., A. Germann, J. Gebert, and S. Dihlmann. 2010. Restoration of absent in melanoma 2 (AIM2) induces G2/M cell cycle arrest and promotes invasion of colorectal cancer cells. *Int. J. Cancer.* 126:1838–1849.
- Rakoff-Nahoum, S., and R. Medzhitov. 2007. Regulation of spontaneous intestinal tumorigenesis through the adaptor protein MyD88. *Science.* 317:124–127. doi:10.1126/science.1140488
- Rakoff-Nahoum, S., J. Paglino, F. Eslami-Varzaneh, S. Edberg, and R. Medzhitov. 2004. Recognition of commensal microflora by toll-like receptors is required for intestinal homeostasis. *Cell.* 118:229–241. doi:10.1016/j.cell.2004.07.002
- Reddy, B.S., J.H. Weisburger, T. Narisawa, and E.L. Wynder. 1974. Colon carcinogenesis in germ-free rats with 1,2-dimethylhydrazine and N-methyl-n'-nitro-N-nitrosoguanidine. *Cancer Res.* 34:2368–2372.
- Siegmund, B., H.A. Lehr, G. Fantuzzi, and C.A. Dinarello. 2001. IL-1 beta -converting enzyme (caspase-1) in intestinal inflammation. *Proc. Natl. Acad. Sci. USA.* 98:13249–13254. doi:10.1073/pnas.231473998
- Sutterwala, F.S., Y. Ogura, M. Szczepanik, M. Lara-Tejero, G.S. Lichtenberger, E.P. Grant, J. Bertin, A.J. Coyle, J.E. Galán, P.W. Askenase, and R.A. Flavell. 2006. Critical role for NALP3/CIAS1/Cryopyrin in innate and adaptive immunity through its regulation of caspase-1. *Immunity.* 24:317–327. doi:10.1016/j.immuni.2006.02.004
- Taxman, D.J., J. Zhang, C. Champagne, D.T. Bergstralh, H.A. Jocca, J.D. Lich, and J.P. Ting. 2006. Cutting edge: ASC mediates the induction of multiple cytokines by *Porphyromonas gingivalis* via caspase-1-dependent and -independent pathways. *J. Immunol.* 177:4252–4256.
- Uronis, J.M., H.H. Herfarth, T.C. Rubinas, A.C. Bissahoyo, K. Hanlon, and D.W. Threadgill. 2007. Flat colorectal cancers are genetically determined and progress to invasion without going through a polypoid stage. *Cancer Res.* 67:11594–11600. doi:10.1158/0008-5472.CAN-07-3242
- Uronis, J.M., M. Mühlbauer, H.H. Herfarth, T.C. Rubinas, G.S. Jones, and C. Jobin. 2009. Modulation of the intestinal microbiota alters colitis-associated colorectal cancer susceptibility. *PLoS One.* 4:e6026. doi:10.1371/journal.pone.0006026
- Villani, A.C., M. Lemire, G. Fortin, E. Louis, M.S. Silverberg, C. Collette, N. Baba, C. Libioulle, J. Belaiche, A. Bitton, et al. 2009. Common variants in the NLRP3 region contribute to Crohn's disease susceptibility. *Nat. Genet.* 41:71–76. doi:10.1038/ng.285
- Zitvogel, L., A. Tesniere, and G. Kroemer. 2006. Cancer despite immunosurveillance: immunoselection and immunosubversion. *Nat. Rev. Immunol.* 6:715–727. doi:10.1038/nri1936